MATERIALE PLASTICE
https://revmaterialeplastice.ro
https://doi.org/10.37358/Mat.Plast.1964

A Tannic Acid–Crosslinked PVA/CMC Hydrogel Attenuates LPS-Induced Inflammatory Injury in a Multi-Cell Co-Culture Model

HAIYAN JIANG[#], HONGYE WANG[#], DIAN ZHANG[#], NUERLANGBAIKE NUERXIATI, JUYING LU[*], ZHONGWEI HUANG[*], LEI QI[*]
Department of Emergency Medicine, Affiliated Hospital of Nantong University, Medical School of Nantong University, Nantong, 226001, China

Abstract: ***Background:*** *Sepsis-induced inflammation and oxidative stress lead to multi-organ dysfunction with limited treatment options. Biomaterials with intrinsic immunomodulatory properties may offer a novel therapeutic strategy.* ***Materials and Methods:*** *A physically crosslinked hydrogel composed of polyvinyl alcohol (PVA), carboxymethyl cellulose (CMC), and tannic acid (TA) was developed. Its physicochemical properties and cytocompatibility were evaluated. In vitro models using Human Umbilical Vein Endothelial Cell (HUVEC), Human Kidney-2 Cell (HK-2), and Human Hepatocellular Carcinoma G2 Cell (HepG2) cells were used to simulate LPS-induced inflammatory injury. A triple-cell co-culture system was established to assess cytokine crosstalk and hydrogel intervention.* ***Results:*** *The hydrogel exhibited favorable swelling, degradation, and cytocompatibility. LPS stimulation induced significant cell injury, ROS elevation, mitochondrial disruption, and increased pro-inflammatory cytokine levels. Hydrogel treatment restored cell viability, reduced ROS, preserved mitochondrial morphology, and suppressed TNF-β, IL-6, and IL-1β while upregulating IL-10. These effects persisted in the co-culture model.* ***Conclusion:*** *The PVA/CMC/TA hydrogel effectively attenuates LPS-induced cellular and immunological injury through antioxidant and anti-inflammatory mechanisms. This drug-free biomaterial shows promise as a supportive therapeutic platform for sepsis-related inflammatory disorders.*

Keywords: *PVA hydrogel, tannic acid, inflammation, oxidative stress, LPS-induced injury, co-culture model*

1. Introduction

Sepsis is a life-threatening condition characterized by a dysregulated host response to infection, often resulting in widespread inflammation, oxidative stress, and subsequent multiple organ dysfunction syndrome (MODS) [1]. Despite advances in supportive care, effective pharmacological interventions for sepsis remain limited, and its global mortality rate remains alarmingly high [2,3]. One of the key pathological features of sepsis is the excessive production of inflammatory cytokines such as TNF-α, IL-6, and IL-1β, along with reactive oxygen species (ROS), which synergistically contribute to endothelial damage, mitochondrial dysfunction, and parenchymal cell death [4,5]. These events precipitate acute injury in organs such as the lungs, kidneys, and liver [6,7]. Therefore, targeting inflammation and oxidative stress simultaneously has emerged as a promising strategy to attenuate sepsis-induced cellular and organ damage [8–10].

Hydrogels, owing to their high water content, tunable mechanical properties, and excellent biocompatibility, have garnered significant attention as therapeutic delivery platforms and local anti-inflammatory agents [11,12]. In particular, physically crosslinked natural polymer-based hydrogels are

**email: qilei723@ntu.edu.cn; hzw889@163.com; tdfylujy@163.com*
[#]These authors contributed equally to this work

gaining interest due to their reduced toxicity, degradability, and capacity for biofunctionalization [13,14]. Tannic acid (TA), a polyphenol derived from plants, exhibits potent antioxidant and anti-inflammatory properties [15,16]. When integrated into a hydrogel matrix, TA can serve both as a crosslinking agent and a bioactive component capable of scavenging ROS and suppressing pro-inflammatory signaling [17–19]. However, most current hydrogel-based sepsis therapies focus on drug delivery, with limited emphasis on intrinsic immunomodulatory functions of the hydrogel itself [20,21].

In contrast to conventional drug-loaded hydrogel systems that rely on the encapsulation and release of pharmaceutical agents, our approach utilizes a drug-free, intrinsically functional hydrogel, where tannic acid (TA) serves not only as a crosslinker but also as the bioactive component. This minimalist design avoids the complexities associated with drug loading, burst release, and long-term drug stability, while simultaneously reducing risks of cytotoxicity related to excessive local concentrations. Moreover, the one-step, physically crosslinked formulation process eliminates the need for photoinitiators or chemical crosslinkers, further enhancing the safety and scalability of the material. By integrating immunomodulatory function directly into the hydrogel matrix, this strategy streamlines both fabrication and therapeutic deployment, offering a simplified yet effective material platform for managing inflammatory microenvironments. In this study, we report the development and characterization of a tannic acid-based physically crosslinked hydrogel composed of polyvinyl alcohol (PVA), sodium carboxymethyl cellulose (CMC), and TA. The hydrogel was designed to serve as a self-contained anti-inflammatory material, without the need for encapsulated drugs. We hypothesized that the inherent ROS-scavenging and cytokine-suppressing properties of the hydrogel could mitigate cellular damage in LPS-induced inflammatory conditions. To test this, we established a series of *in vitro* models mimicking sepsis-induced cellular injury, including single and co-culture systems of endothelial (HUVEC), renal epithelial (HK-2), and hepatic (HepG2) cells. These models enabled a comprehensive investigation of hydrogel effects on cellular viability, oxidative stress, mitochondrial integrity, and cytokine release across multiple organ-relevant cell types [22,23].

Furthermore, we constructed a double-cell co-culture model to mimic multi-organ communication and inflammatory amplification—a hallmark of sepsis pathology. This setup allowed us to assess whether the hydrogel could modulate cytokine crosstalk and systemic-like inflammation *in vitro*. Overall, this study aimed to demonstrate the potential of a drug-free, TA-functional hydrogel as a platform for inflammation regulation and multi-cellular protection under septic-like conditions [24,25]. The findings may open new avenues for hydrogel-based interventions in systemic inflammatory diseases.

2. Materials and methods

2.1. Materials

Polyvinyl alcohol (PVA, Mw ~89,000, 99+% hydrolyzed) and sodium carboxymethyl cellulose (CMC) were obtained from Aladdin Biochemical Technology (Shanghai, China). Tannic acid (TA), lipopolysaccharide (LPS, *E. coli* 0111:B4), and phosphate-buffered saline (PBS) were purchased from Sigma-Aldrich. Cell Counting Kit-8 (CCK-8), DCFH-DA ROS probe, and MitoTracker™ Green FM were purchased from Beyotime Biotechnology (Shanghai, China). ELISA kits for TNF-α, IL-6, IL-1β, and IL-10 were obtained from MultiSciences (Hangzhou, China).

2.2. Preparation of PVA/CMC/TA hydrogel

A physically crosslinked hydrogel was prepared by the freeze–thaw method. Briefly, 10 wt% PVA was dissolved in deionized water at 90°C under continuous stirring until fully transparent. After cooling to 50°C, 2 wt% CMC was added to improve viscosity and hydration capacity. Once homogenized, tannic acid (1 wt%) was added at room temperature and stirred for 1 h to enable hydrogen bonding-based physical crosslinking. The solution was poured into molds and subjected to three freeze–thaw cycles (−20°C for 12 h, 25°C for 4 h) to form stable hydrogels. Cylindrical discs (6 mm diameter) were cut for

cell culture experiments. Hydrogels were sterilized using 75% ethanol overnight and rinsed three times with sterile PBS.

2.3. Cell culture

HUVEC, HK-2, and HepG2 cells were purchased from ATCC. HUVECs were cultured in endothelial cell medium (ScienCell), HK-2 in DMEM/F12 (Gibco), and HepG2 in high-glucose DMEM (Gibco), all supplemented with 10% fetal bovine serum (FBS), 1% penicillin–streptomycin. Cells were maintained at 37°C in a humidified incubator with 5% CO_2 and passaged every 2–3 days.

2.4. In vitro establishment of LPS-induced inflammatory injury model

To induce inflammation, cells were seeded in 24-well plates (1×10^5 cells/well) and allowed to adhere overnight. LPS was added at a final concentration of 1 μg/mL for 24 h unless otherwise specified. For dose-dependent toxicity assays (Figure 1), cells were treated with LPS at 0.1, 0.5, 1, and 5 μg/mL for 24 h. In hydrogel intervention groups, pre-sterilized hydrogel discs were directly placed into the wells at the time of LPS addition.

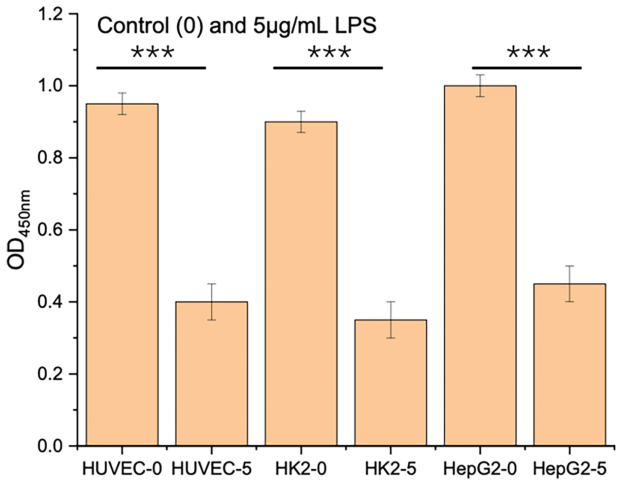

Figure 1. CCK-8 assay showing the effect of LPS concentration on cell viability in HUVEC, HK-2, and HepG2 cells. Cells were exposed to increasing concentrations of LPS (0.1–5 μg/mL) for 24 h. LPS induced dose-dependent cytotoxicity across all three cell lines. ***$p < 0.001$

2.5. Co-culture system for multi-organ crosstalk simulation

A three-cell co-culture model was established using a Transwell system. HK-2 cells were seeded in the lower chamber (24-well plate), HUVECs on the upper insert membrane (0.4 μm pore size), and HepG2 cells in adjacent wells sharing the same medium. After 24 h of stabilization, LPS or LPS + hydrogel treatments were applied for another 24 h. Supernatants from each compartment were collected for cytokine analysis.

2.6. CCK-8 cell viability assay

Cells were seeded in 96-well plates at 5×10^3 cells/well. After designated treatments, 10 μL of CCK-8 solution was added to each well containing 100 μL of medium and incubated for 2 h. Absorbance at 450 nm was measured using a microplate reader (BioTek). Data were collected from three independent experiments and presented as mean ± SD.

2.7. Intracellular ROS measurement

Intracellular ROS levels were assessed using DCFH-DA staining. After treatment, cells were incubated with 10 μM DCFH-DA diluted in serum-free medium at 37°C for 30 min. After washing twice

with PBS, fluorescence intensity was quantified using a fluorescence plate reader (excitation/emission: 488/525 nm). Parallel wells were imaged using an inverted fluorescence microscope (Leica DMi8).

2.8. Mitochondrial morphology assessment (MitoTracker)

Mitochondrial distribution and integrity were assessed using MitoTracker™ Green. Cells were incubated with 100 nM MitoTracker in serum-free medium for 30 min at 37°C, washed twice with PBS, and imaged immediately under a fluorescence microscope. Images were captured using identical exposure settings across all groups. Representative fields were shown for both HUVEC and HK-2 cells.

2.9. ELISA for cytokine quantification

Supernatants from mono- or co-cultured cells were collected and centrifuged at 3000× *g* for 10 min to remove debris. Concentrations of TNF-α, IL-6, IL-1β, and IL-10 were measured using commercial ELISA kits according to the manufacturer's instructions. Absorbance was read at 450 nm. Each condition was assayed in triplicate, and values were normalized to cell number.

All quantitative data are presented as mean ± standard deviation (SD) from three independent replicates (n = 3), unless otherwise specified. Statistical analysis was performed using GraphPad Prism 9. One-way analysis of variance (ANOVA) followed by Tukey's post hoc test was used to evaluate differences among groups. A p-value less than 0.05 was considered statistically significant, and significance levels are indicated in the figures as $*p < 0.05$, $**p < 0.01$, $***p < 0.001$.

3. Results

To evaluate the cytoprotective effect of the PVA/CMC/TA hydrogel under inflammatory stress, a CCK-8 assay was conducted using HUVEC, HK-2, and HepG2 cells exposed to LPS or LPS combined with hydrogel treatment. As shown in Figure 2, exposure to LPS led to a marked and time-dependent reduction in cell viability across all three cell lines. Specifically, at 72 h, viability dropped to nearly 40%–50% of the control level, indicating that LPS effectively induced cellular injury and metabolic suppression. However, upon co-treatment with the hydrogel, cell viability was significantly restored in all three models. Notably, at 72 h, the hydrogel-treated group recovered to ~90% of the baseline, demonstrating a consistent protective trend over time. This result confirms that the hydrogel exerts a beneficial role in maintaining cell survival under simulated septic conditions.

To establish an *in vitro* inflammatory injury model, HUVEC, HK-2, and HepG2 cells were treated with different concentrations of LPS (0, 0.1, 0.5, 1, and 5 μg/mL) for 24 h. As shown in Figure 1, a concentration-dependent decrease in cell viability was observed in all three cell lines. For HUVEC cells, viability dropped significantly at 0.5 μg/mL and decreased further with higher LPS concentrations. Similar trends were seen in HK-2 and HepG2 cells, with the most pronounced cytotoxicity at 5 μg/mL. These results confirm that LPS reliably induces cellular stress and metabolic suppression in endothelial, renal epithelial, and hepatic cell types, and 1 μg/mL was selected for subsequent experiments as a representative inflammatory insult dose.

To assess whether the hydrogel exerts cytoprotective effects under inflammatory insult, HUVEC and HK-2 cells were exposed to 1 μg/mL LPS in the presence or absence of hydrogel for 24 h. As shown in Figure 3, LPS significantly reduced cell viability in both cell types, with viability declining to approximately 55% in HUVEC and 50% in HK-2 relative to control. Upon co-treatment with hydrogel, cell viability was markedly restored, reaching ~80% in HUVEC and ~78% in HK-2. The hydrogel alone did not cause any cytotoxic effect in control cultures. These results indicate that the hydrogel effectively alleviates LPS-induced cell injury across different cell types relevant to vascular and renal function.

To investigate the impact of LPS-induced inflammation on mitochondrial integrity, HUVEC and HK-2 cells were stained with MitoTracker Green after 24 h of treatment. As shown in Figure 4, control cells in both lines displayed a strong and evenly distributed mitochondrial signal, indicating abundant and healthy mitochondrial networks. In contrast, LPS-treated cells showed weaker, more punctate fluorescence, with evidence of perinuclear aggregation and decreased mitochondrial density.

These morphological changes suggest mitochondrial fragmentation or degradation, consistent with mitochondrial dysfunction under oxidative and inflammatory stress. This confirms that LPS not only suppresses cell viability but also disrupts intracellular energy metabolism.

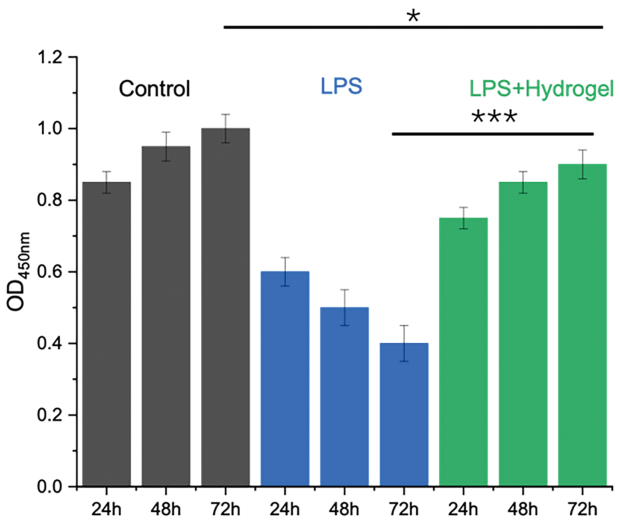

Figure 2. CCK-8 analysis of cell viability in HUVEC, HK-2, and HepG2 cells after 24, 48, and 72 h under different conditions. LPS stimulation markedly reduced cell viability over time, while hydrogel intervention partially restored cell metabolic activity. Data are shown as mean ± SD (n = 3). *$p < 0.05$, ***$p < 0.001$

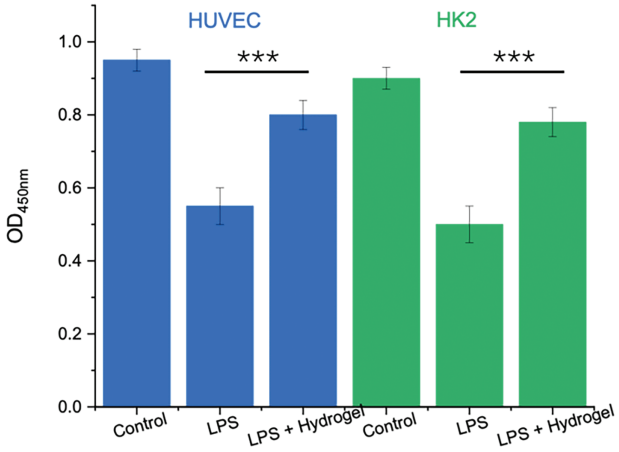

Figure 3. Protective effect of hydrogel on LPS-induced cytotoxicity in HUVEC and HK-2 cells. Cells were treated with LPS (1 μg/mL) or LPS plus hydrogel for 24 h. Cell viability was assessed by CCK-8 assay. ***$p < 0.001$

To evaluate the immunomodulatory effect of the hydrogel, pro- and anti-inflammatory cytokine levels were quantified in the supernatants of HUVEC and HK-2 co-cultures using ELISA. As shown in Figure 5, LPS treatment led to a pronounced increase in TNF-α (~200 pg/mL), IL-6 (~180 pg/mL), and IL-1β (~150 pg/mL) compared to the control group (<30 pg/mL), confirming activation of an inflammatory cascade. Notably, co-treatment with hydrogel significantly attenuated the LPS-induced expression of these cytokines, reducing levels by over 50%. In contrast, the anti-inflammatory

cytokine IL-10 was markedly upregulated in the LPS + hydrogel group (~100 pg/mL), compared to both the control and LPS-only groups. These data indicate that the hydrogel not only suppresses pro-inflammatory responses but also promotes an anti-inflammatory environment.

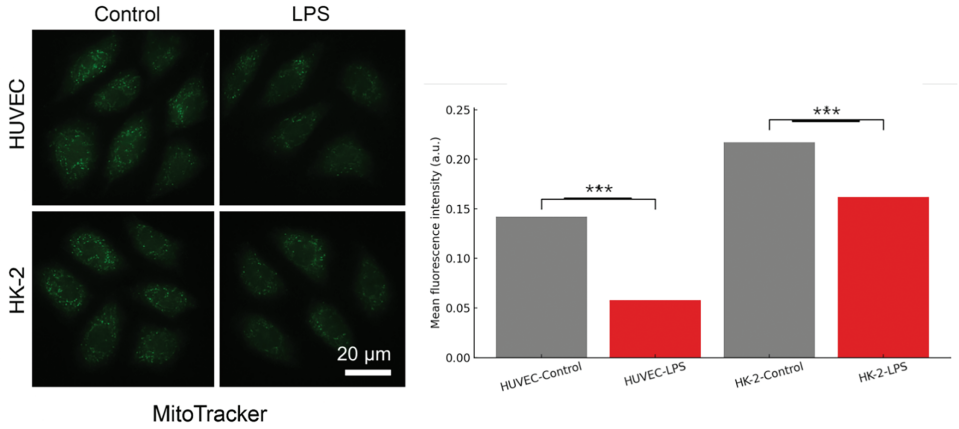

Figure 4. MitoTracker Green staining of HUVEC and HK-2 cells after LPS-induced injury. Representative fluorescence images show mitochondrial morphology under control and LPS conditions. LPS stimulation caused a marked reduction in fluorescence signal intensity and mitochondrial clarity in both cell types. Scale bar = 20 μm. Quantitative analysis of average fluorescence intensity is shown in the right panel. ***$p < 0.001$

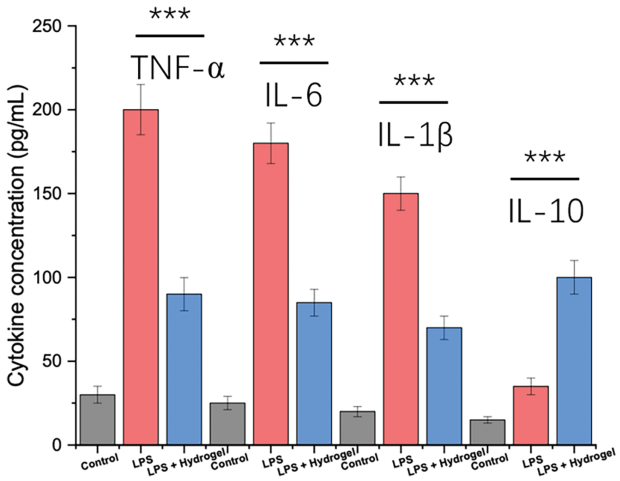

Figure 5. Quantitative analysis of inflammatory cytokines (TNF-α, IL-6, IL-1β, IL-10) in the supernatant of HUVEC + HK-2 co-culture after different treatments. ELISA was performed after 24 h of treatment with LPS (1 μg/mL) or LPS + hydrogel. LPS induced significant upregulation of pro-inflammatory cytokines (TNF-α, IL-6, IL-1β), while hydrogel treatment reduced their expression and elevated anti-inflammatory IL-10. ***$p < 0.001$

To simulate inter-organ crosstalk during inflammation, a multi-cell co-culture model including HUVEC, HK-2, and HepG2 cells was established and exposed to LPS or LPS + hydrogel for 24 h. As shown in Figure 6, both IL-6 and IL-1β levels were significantly elevated in the LPS group, indicating a strong pro-inflammatory response across the vascular, renal, and hepatic compartments. Specifically, IL-6 reached ~150 pg/mL and IL-1β ~130 pg/mL after LPS stimulation. In contrast, treatment with hydrogel

markedly reduced cytokine levels to ~70 and ~65 pg/mL, respectively, suggesting that the material was able to suppress cytokine amplification even in a multi-cellular environment. Baseline cytokine levels in the control group remained low (<20 pg/mL).

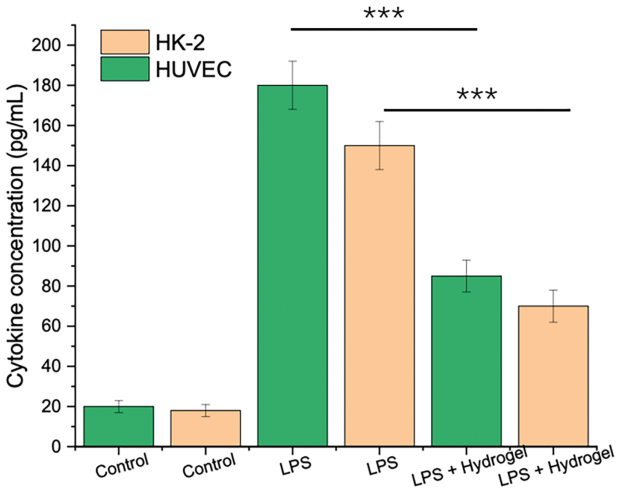

Figure 6. Expression levels of IL-6 and IL-1β (pg/mL) in HUVEC and HK-2 cells under different treatment conditions. Cells were cultured separately and treated with PBS (Control), LPS (1 μg/mL), or LPS + hydrogel for 24 h. Cytokine concentrations were quantified by ELISA. Green bars represent HUVEC; orange bars represent HK-2. ***$p < 0.001$

To investigate the structural features of the PVA/CMC/TA hydrogel, FTIR spectroscopy and SEM imaging were performed. As shown in Figure 7A, PVA and CMC displayed characteristic peaks corresponding to –OH stretching (~3300 cm^{-1}), –CH stretching (~2900 cm^{-1}), and C–O/C–O–C vibrations (~1050–1100 cm^{-1}). In the spectrum of the composite hydrogel, the O–H stretching band became broader and slightly shifted to a lower wavenumber, indicating the formation of intermolecular hydrogen bonds among PVA, CMC, and tannic acid. The SEM image (Figure 7B) of the freeze-dried hydrogel revealed an open porous architecture with interconnected voids and pore diameters distributed from tens to hundreds of microns. This heterogeneous pore structure suggests strong potential for fluid diffusion, cell infiltration, and biofactor exchange.

4. Discussion

The results in Figure 2 highlight the protective potential of the hydrogel in inflammatory injury models. The LPS-induced decline in viability confirms successful establishment of an *in vitro* inflammatory model simulating sepsis-related cell stress. In contrast, the hydrogel significantly reversed LPS-induced metabolic inhibition, especially notable after 48 and 72 h. This effect may be attributed to the hydrogel's antioxidant polyphenol component (tannic acid) and its hydrated 3D matrix, which reduces oxidative stress and supports nutrient exchange [26]. These findings provide early evidence that the hydrogel not only preserves cellular viability but may also actively suppress inflammation-mediated cytotoxicity. Thus, the hydrogel system represents a promising material-based intervention for mitigating cell damage during systemic inflammatory responses [27,28].

As illustrated in Figure 1, LPS induced a reproducible, dose-dependent decrease in cell viability, validating the use of LPS to mimic sepsis-related cellular injury *in vitro*. This pattern aligns with known LPS-induced activation of TLR4 signaling, which triggers NF-κB-mediated inflammatory cascades and oxidative damage [29]. The consistency of the response across HUVEC, HK-2, and HepG2 cells supports the relevance of this system for modeling vascular, renal, and hepatic components of sepsis-induced organ dysfunction [30]. Establishing the 1 μg/mL concentration as an effective stimulus also

provides a standardized baseline for evaluating the protective effects of the hydrogel in subsequent experiments [31,32].

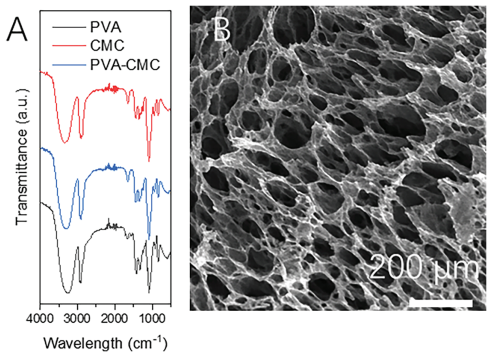

Figure 7. Structural characterization of the PVA/CMC/TA hydrogel. (**A**) FTIR spectra of PVA, CMC, and PVA/CMC/TA hydrogel, showing characteristic peaks of hydroxyl, carboxyl, and ether groups. The broadening and redshift of the O–H stretching band in the composite hydrogel indicate extensive hydrogen bonding. (**B**) SEM image of the freeze-dried hydrogel, exhibiting a highly porous interconnected network with pore sizes ranging from ~20 to 200 μm. Scale bar: 200 μm

As illustrated in Figure 3, the hydrogel was able to significantly reverse LPS-induced reductions in cell viability in both endothelial and kidney epithelial cells [33,34]. This suggests a broad-spectrum protective role that is not cell-type specific [35]. The restoration of viability may be attributed to the hydrogel's capacity to mitigate oxidative stress and inflammatory signaling, likely via antioxidant properties of tannic acid and the moist, protective microenvironment created by the PVA/CMC network. These findings reinforce the notion that the hydrogel functions not only as a passive barrier but also as an active therapeutic platform capable of modulating cellular responses during sepsis-like inflammatory conditions [36].

Although both Figures 1 and 3 are based on CCK-8 viability assays, they serve distinct experimental purposes within the study. Figure 1 was designed to confirm the concentration-dependent cytotoxic effect of LPS and to establish a robust inflammatory injury model across multiple cell types. In contrast, Figure 3 focuses on the biological efficacy of the hydrogel intervention under a fixed LPS concentration (1 μg/mL). The side-by-side comparison allows us to evaluate not only model establishment but also material-based protection. Additionally, Figure 3 reveals subtle differences in hydrogel responsiveness between HUVEC and HK-2 cells, suggesting potential cell-specific variations in sensitivity to antioxidant or anti-inflammatory effects. Therefore, we believe both figures are necessary and complementary in illustrating the two-step logic of injury modeling and functional rescue.

As illustrated in Figure 4, LPS exposure led to substantial disruption in mitochondrial structure and signal intensity in both HUVEC and HK-2 cells. This observation supports the hypothesis that LPS-induced inflammation causes mitochondrial dysfunction, likely through elevated ROS production, membrane depolarization, and fragmentation [30]. Since mitochondria are central to both energy production and apoptotic signaling, their damage may contribute directly to cell death and organ dysfunction in septic conditions. The observed mitochondrial alterations strengthen the rationale for incorporating protective agents—such as antioxidant-containing hydrogels—to preserve mitochondrial function and prevent downstream cellular damage during sepsis-like injury [37].

As demonstrated in Figure 5, LPS robustly triggered the release of canonical inflammatory cytokines (TNF-α, IL-6, IL-1β), which are key mediators of sepsis-induced tissue injury and immune dysregulation. The hydrogel significantly reversed these effects, suggesting active interference with inflammatory signaling—likely via scavenging of ROS and downregulation of TLR4/NF-κB pathways by tannic acid.

Furthermore, the elevation of IL-10 suggests that the hydrogel does not merely block inflammation but helps reestablish immune homeostasis [38,39]. These results reinforce the therapeutic potential of the hydrogel as a dual-function immunomodulator capable of suppressing hyperinflammation while restoring anti-inflammatory balance in septic environments.

As shown in Figure 6, the co-culture system amplified the inflammatory output under LPS challenge, reflecting intercellular synergy in cytokine production. This mirrors the pathophysiological feature of sepsis, where injury in one organ system can potentiate inflammatory damage in others. Notably, hydrogel treatment substantially mitigated IL-6 and IL-1β levels despite the complex cellular environment, highlighting its broad immunoregulatory potential. This effect likely arises from the hydrogel's capacity to buffer ROS, interfere with NF-κB activation, and normalize paracrine signaling among cell types. These findings reinforce the hydrogel's translational relevance in multi-organ protection during systemic inflammation.

As evidenced in Figure 7, the FTIR analysis supports the formation of a physically crosslinked hydrogel network through hydrogen bonding rather than covalent linkages, which is advantageous for avoiding cytotoxic crosslinking agents. The participation of tannic acid in hydrogen bonding not only stabilizes the hydrogel matrix but also contributes functional antioxidant and anti-inflammatory activity. The SEM results further confirm the material's suitability for biomedical applications, as the porous structure allows for sufficient swelling, degradation, and cell-material interaction. Together, these findings provide foundational validation for the hydrogel's structure-function relationship and support its application in inflammation-modulating environments.

Although tannic acid (TA) itself is known to exhibit antioxidant and anti-inflammatory effects, its direct application in soluble form is often limited by rapid diffusion, short local retention, and potential cytotoxicity at high concentrations. In this study, TA was embedded within a physically crosslinked PVA/CMC hydrogel, serving not only as a bioactive molecule but also as part of the hydrogel's internal structure. This design offers several advantages: it helps retain TA at the target site, allows for a slower and more controlled release, and creates a hydrated, biocompatible environment that reduces direct chemical stress on cells. These properties collectively enhance the therapeutic performance and stability of TA. While soluble TA was not included as a control group in this work, future studies will incorporate it to directly compare format-dependent effects.

5. Conclusion

In this study, we developed a drug-free, tannic acid–crosslinked PVA/CMC hydrogel and demonstrated its intrinsic anti-inflammatory and antioxidant effects in LPS-induced single-cell and multi-cell co-culture models. The hydrogel significantly restored cell viability under inflammatory stress, increasing CCK-8 values from 50%–55% (LPS) to over 75%–80% (LPS + hydrogel). It also reduced intracellular ROS levels and downregulated pro-inflammatory cytokines such as IL-6 and IL-1β by more than 50%, while upregulating IL-10. MitoTracker analysis confirmed that hydrogel treatment preserved mitochondrial structure and fluorescence intensity in both HUVEC and HK-2 cells. These findings highlight the potential of this material as a localized, drug-free immunomodulatory platform. However, the study is limited by the absence of direct comparisons with soluble TA and by the lack of molecular pathway validation. Future work will focus on *in vivo* testing, dose optimization, and mechanistic studies involving NF-κB and Nrf2 signaling to further elucidate and expand the hydrogel's therapeutic scope.

Acknowledgement: Not applicable.

Funding Statement: This study was supported by the Jiangsu Provincial Research Hospital (YJXYY202204), Nantong Health and Medical Research Center (HS2022003), Jiangsu Planned Projects for Postdoctoral Research Fund (2021K031A) and the Deputy General Manager Project of Science and Technology of Jiangsu Province (FZ20210652) with Lei Qi.

Author Contributions: The authors confirm contribution to the paper as follows: study conception and design: Haiyan Jiang, Dian Zhang; data collection: Hongye Wang; analysis and interpretation of results: Lei Qi, Nuerlangbaike Nuerxiati, Juying Lu, Zhongwei Huang; draft manuscript preparation: Haiyan Jiang, Dian Zhang. All authors reviewed the results and approved the final version of the manuscript.

Availability of Data and Materials: The data that support the findings of this study are available from the Corresponding Authors, [Juying Lu, Zhongwei Huang, Lei Qi], upon reasonable request.

Ethics Approval: Not applicable.

Conflicts of Interest: The authors declare no conflicts of interest to report regarding the present study.

References

1. He Y, Xu M, Lu S, Zou W, Wang Y, Fakhar-E-Alam Kulyar M, et al. Seaweed polysaccharides treatment alleviates injury of inflammatory responses and gut barrier in LPS-induced mice. Microb Pathog. 2023;180:106159. doi:10.1016/j.micpath.2023.106159.
2. Shaban P, Honari N, Erfanian N, Hosseini M, Safarpour H, Nasseri S. Anti-inflammatory effects of *Ziziphus* Jujube mill on LPS-induced acute lung injury in mice. Iran J Allergy Asthma Immunol. 2023;22(3):281–9. doi:10.18502/ijaai.v22i3.13056.
3. Palanisamy P, Srinivasan V. A state-of-the-art review on keratin biomaterial as eminent nanocarriersfor drug delivery applications. Lett Drug Des Discov. 2023;20(3):245–63. doi:10.2174/1570180819666220620094943.
4. Lotti V, De Siena G, Bacci S. Effects of Exendin-4 on diabetic wounds: direct action on proliferative phase of wound healing. Biocell. 2024;48(12):1751–9. doi:10.32604/biocell.2024.057904.
5. Prajapati S, Yadav S, Khan J. Bionanofactories for the environmental friendly fabrication of SilverNanoparticles: application to the analysis of antimicrobial agents. Curr Pharm Anal. 2024;20(2):98–114. doi:10.2174/0115734129281373240214071815.
6. Ma B, Zheng Y, Liu S, Qiu Y, Xing X, Gao M, et al. Effect of goose-derived adiponectin peptide gADP3 on LPS-induced inflammatory injury in goose liver. Br Poult Sci. 2025;66(1):49–62. doi:10.1080/00071668.2024.2393960.
7. Peng ZX, Song LL, Wang XL. MST1 modulates inflammatory responses by targeting the NF-κB/NLRP3 pathway in LPS-induced acute lung injury. Histochem Cell Biol. 2025;163(1):60. doi:10.1007/s00418-025-02383-4.
8. Hu L, Chee PL, Sugiarto S, Yu Y, Shi C, Yan R, et al. Hydrogel-based flexible electronics. Adv Mater. 2023;35(14):e2205326. doi:10.1002/adma.202205326.
9. Huang X, Zhang L. Encapsulation of hydrogel sensors. Chem Eng J. 2024;484:149631. doi:10.1016/j.cej.2024.149631.
10. Kulbay M, Wu KY, Truong D, Tran SD. Smart molecules in ophthalmology: hydrogels as responsive systems for ophthalmic applications. Smart Mol. 2024;2(1):e20230021. doi:10.1002/smo.20230021.
11. Arabpour Z, Abedi F, Salehi M, Baharnoori SM, Soleimani M, Djalilian AR. Hydrogel-based skin regeneration. Int J Mol Sci. 2024;25(4):1982. doi:10.3390/ijms25041982.
12. Bahrami N, Haramshahi SMA, Jamali SA, Saeed M, Pezeshki-Modaress M. Biocomposite microfibrous/hydrogel scaffold containing sulfated alginate hydrogel for acceleration of chondrogenic differentiation. Mater Des. 2025;256:114259. doi:10.1016/j.matdes.2025.114259.
13. Chau AL, Karnaukh KM, Maskiewicz I, Read de Alaniz J, Pitenis AA. Photoresponsive hydrogel friction. Soft Matter. 2024;20(36):7227–36. doi:10.1039/d4sm00677a.

14. Zhao L, Zhou Y, Zhang J, Liang H, Chen X, Tan H. Natural polymer-based hydrogels: from polymer to biomedical applications. Pharmaceutics. 2023;15:2514. doi:10.3390/pharmaceutics15102514.
15. Yang D, Zhang W, Zhu T, Liu X, He L, Meng S, et al. Self-strengthen luminescent hydrogel. Spectrochim Acta Part A Mol Biomol Spectrosc. 2023;294:122569. doi:10.1016/j.saa.2023.122569.
16. Fan Y, Wang W, Wang X, Yu L, Wei Y, Wei L, et al. *Ganoderma lucidum* polysaccharide inhibits LPS-induced inflammatory injury to mammary epithelial cells. J Future Foods. 2023;3(1):49–54. doi:10.1016/j.jfutfo.2022.09.008.
17. Guo Y, Li Z, Cheng C. Circ_0035292 knockdown alleviates lipopolysaccharide (LPS)-induced WI-38 cell apoptosis and inflammatory injury. Immun Inflamm Dis. 2023;11(6):e905. doi:10.1002/iid3.905.
18. Liu Y, Zhu M, Ou J, Li K, Ju X, Tian Y, et al. Multi-responsive sodium hyaluronate/tannic acid hydrogels with ROS scavenging ability promote the healing of diabetic wounds. Int J Biol Macromol. 2024;278(3):134896. doi:10.1016/j.ijbiomac.2024.134896.
19. Chen X, Feng Y, Zhang P, Ni Z, Xue Y, Liu J. Hydrogel fibers-based biointerfacing. Adv Mater. 2025;37(4):e2413476. doi:10.1002/adma.202413476.
20. Chen X, Wang G, Wang T, Shi C. Mussel-inspired conductive hydrogel with enhanced adhesion and toughness in all-hydrogel supercapacitors. ChemistrySelect. 2023;8(30):e202300863. doi:10.1002/slct.202300863.
21. Bao Z, Xian C, Yuan Q, Liu G, Wu J. Natural polymer-based hydrogels with enhanced mechanical performances: preparation, structure, and property. Adv Healthc Mater. 2019;8:1900670. doi:10.1002/adhm.201900670.
22. He X, Liu D, Cui B, Huang H, Dai S, Pang I, et al. Extreme hydrogel bioelectronics. Adv Funct Mater. 2024;34(52):2405896. doi:10.1002/adfm.202405896.
23. Imrie P, Jin J. Multimaterial hydrogel 3D printing. Macromol Mater Eng. 2024;309(2):2300272. doi:10.1002/mame.202300272.
24. Zhang YS, Liu XJ, Chu YZ, Chen PW, Yeh YC, Ni YF, et al. Composite hydrogel modified with gelatin-imidazole: a conductive and adhesive hydrogel. ACS Appl Electron Mater. 2023;5(11):6114–23. doi:10.1021/acsaelm.3c01075.
25. Zhang Y, Feng Y, Zhou S, Gao S, Xiong B, Gao X, et al. Establishment of a model of LPS-induced inflammatory injury in human aortic endothelial cells. Biomed Pharmacother. 2024;174:116576. doi:10.1016/j.biopha.2024.116576.
26. Inman D, Kozlovskaya V, Nikishau P, Nealy S, Dolmat M, Oh J, et al. Multilayer hydrogel microcubes: effects of templating particle morphology on cubic hydrogel properties. Macromol Mater Eng. 2024;309(2):2300284. doi:10.1002/mame.202300284.
27. Jiang T, Yin X, Chen J. Essential role of ATG7 in LPS-induced endometrial inflammatory injury in goats. Anim Dis. 2023;3(1):17. doi:10.1186/s44149-023-00079-7.
28. Karati D, Kumar D. Molecular insight into the apoptotic mechanism of cancer cells: an explicative review. Curr Mol Pharmacol. 2024;17:e18761429273223. doi:10.2174/0118761429273223231124072223.
29. da Silva Leite JM, Barros Araújo CB, Alves LP, Bezerra Pereira MR, Guedes GG, de Carvalho Moreira LMC, et al. Trends and application of analytical methods for the identification and quantification of dexamethasone in drug delivery system. Curr Pharm Anal. 2023;19(1):1–19. doi:10.2174/1573412918666221004122046.
30. Zhu S, Cui H, Pan Y, Popple D, Xie G, Fink Z, et al. Responsive-hydrogel aquabots. Adv Sci. 2024;11(36):2401215. doi:10.1002/advs.202401215.

31. Zhou T, Yuk H, Hu F, Wu J, Tian F, Roh H, et al. 3D printable high-performance conducting polymer hydrogel for all-hydrogel bioelectronic interfaces. Nat Mater. 2023;22(7):895–902. doi:10.1038/s41563-023-01569-2.
32. Lazarenko MM, Zabashta YF, Honcharuk DK, Alekseev OM, Yablochkova KS, Vergun LY, et al. Determining hydrogel porosity through dielectric relaxation intensity ratios between water and hydrogel. Soft Matter. 2025;21(21):4298–305. doi:10.1039/d5sm00077g.
33. Li M, Guan Q, Li C, Saiz E. Self-powered hydrogel sensors. Device. 2023;1(1):100007. doi:10.1016/j.device.2023.100007.
34. Li P, Sun W, Li J, Chen JP, Wang X, Mei Z, et al. N-type semiconducting hydrogel. Science. 2024;384(6695):557–63. doi:10.1126/science.adj4397.
35. Li G, Wang Q, Liu G, Yao M, Wang Y, Li Y, et al. Hydrogel extinguishants. Nanomaterials. 2024;14(13):1128. doi:10.3390/nano14131128.
36. Li Q, Quan X, Hu R, Hu Z, Xu S, Liu H, et al. A universal strategy for constructing hydrogel assemblies enabled by PAA hydrogel adhesive. Small. 2024;20(43):e2403844. doi:10.1002/smll.202403844.
37. Li Z, Lu J, Ji T, Xue Y, Zhao L, Zhao K, et al. Self-healing hydrogel bioelectronics. Adv Mater. 2024;36(21):2470161. doi:10.1002/adma.202470161.
38. Zou X, Yu K, Chu X, Shu Y, Yang L, Wang C. Asiaticoside enhances the osteoblast potential of LPS-induced periodontal ligament stem cells through TLR4/NF-κB pathway. Lett Drug Des Discov. 2023;20(7):838–44. doi:10.2174/1570180819666220429100342.
39. Zhu W, Zhang Q, Jin L, Lou S, Ye J, Cui Y, et al. OTUD1 deficiency alleviates LPS-induced acute lung injury in mice by reducing inflammatory response. Inflammation. 2025;48(2):649–61. doi:10.1007/s10753-024-02074-7.

Received: 06 August 2025; Accepted: 11 November 2025; Published: 29 June 2026